ACS central science

Research Article

Cite This: ACS Cent. Sci. 2018, 4, 1559−1569

http://pubs.acs.org/journal/acscii

Photoinduced Ligand Release from a Silicon Phthalocyanine Dye Conjugated with Monoclonal Antibodies: A Mechanism of Cancer Cell Cytotoxicity after Near-Infrared Photoimmunotherapy

Kazuhide Sato,[†,‡,§] Kanta Ando,[∥] Shuhei Okuyama,[†,⊥] Shiho Moriguchi,[⊥] Tairo Ogura,[⊥] Shinichiro Totoki,[⊥] Hirofumi Hanaoka,[†] Tadanobu Nagaya,[†] Ryohei Kokawa,[⊥] Hideo Takakura,[∥] Masayuki Nishimura,[⊥] Yoshinori Hasegawa,[§] Peter L. Choyke,[†] Mikako Ogawa,[∥] and Hisataka Kobayashi*[,†]

[†]Molecular Imaging Program, Center for Cancer Research, National Cancer Institute, National Institutes of Health, Bethesda, Maryland 20892-1088, United States

[‡]Institute for Advanced Research, Nagoya University, Nagoya, Aichi 464-0814, Japan

[§]Department of Respiratory Medicine, Nagoya University Graduate School of Medicine, Nagoya, Aichi 466-8550, Japan

[∥]Laboratory for Bioanalysis and Molecular Imaging, Graduate School of Pharmaceutical Sciences, Hokkaido University, Sapporo, Hokkaido 060-0812, Japan

[⊥]Shimadzu Corporation, Kyoto 604-8511, Japan

Supporting Information

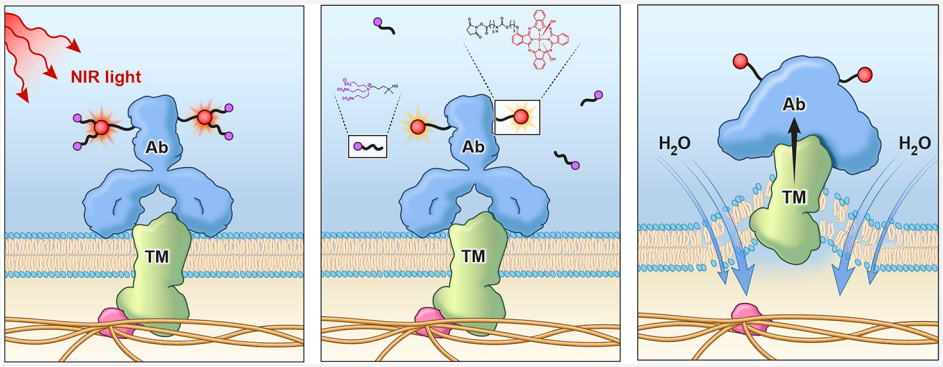

ABSTRACT: Photochemical reactions can dramatically alter physical characteristics of reacted molecules. In this study, we demonstrate that near-infrared (NIR) light induces an axial ligand-releasing reaction, which dramatically alters hydrophilicity of a silicon phthalocyanine derivative (IR700) dye leading to a change in the shape of the conjugate and its propensity to aggregate in aqueous solution. This photochemical reaction is proposed as a major mechanism of cell death induced by NIR photoimmunotherapy (NIR-PIT), which was recently developed as a molecularly targeted cancer therapy. Once the antibody-IR700 conjugate is bound to its target, activation by NIR light causes physical changes in the shape of antibody antigen complexes that are thought to induce physical stress within the cellular membrane leading to increases in transmembrane water flow that eventually lead to cell bursting and necrotic cell death.

INTRODUCTION

Near infrared (NIR) photoimmunotherapy (PIT) is a newly developed, molecularly targeted cancer phototherapy based on conjugating a near-infrared silicon phthalocyanine dye, IRdye700DX (IR700), to a monoclonal antibody (mAb) thereby targeting specific cell-surface molecules.[1−5] A clinical trial with anti-EGFR antibody-IR700-dye conjugate in patients with inoperable head and neck cancer is now entering FDA-designated fast-track global Phase 3 clinical testing (https://clinicaltrials.gov/ct2/show/NCT02422979).

It is known that when antibody-IR700 conjugates are bound to their target cells and are exposed to NIR light, target cells rapidly undergo necrotic/immunogenic cell death (ICD) in a highly selective manner. Real time microscopy demonstrates swelling, blebbing, and bursting of the target cell membrane within minutes of light exposure with minimal damage to adjacent nontarget cells.[6−8] Upon exposure to NIR light, physical stress was thought to be induced within the cellular membrane leading to increases in transmembrane water flow that eventually lead to cell bursting and necrotic cell death.[8] As cytoplasmic contents are rapidly released into the extracellular

Received: August 14, 2018
Published: November 6, 2018

DOI: 10.1021/acscentsci.8b00565
ACS Cent. Sci. 2018, 4, 1559−1569

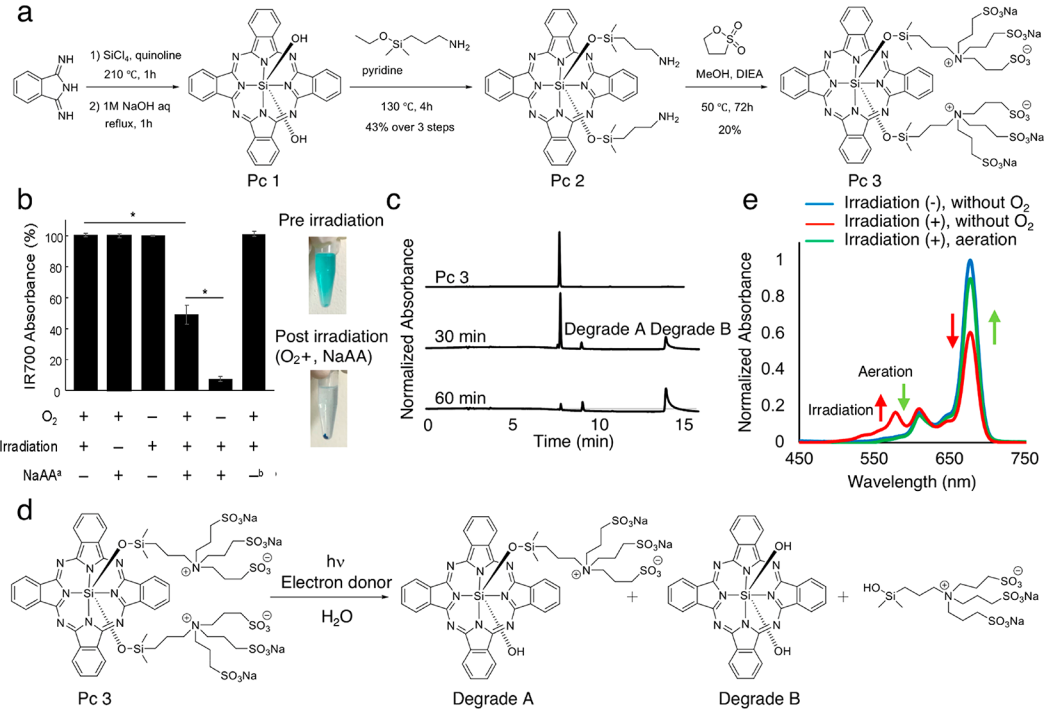

Figure 1. Photolysis analyses of SiPc. (a) Synthetic scheme of **Pc 3**, which has the same axial ligands as IR700. (b) Photolysis analysis. Columns left to right show a decrease in absorbance at 676.5 nm of 1 μM solution of **Pc 3** (PBS, pH 7.5) in oxygenated state with NIR but no NaAA, with NaAA; no irradiation; no deoxygenation, no NaAA; no deoxygenation; deoxygenation or electron acceptor instead of NaAA at 0 and 30 min exposure to 3.5 mW cm^{-2} 676.5 nm light. (footnote a) NaAA = L-ascorbic acid sodium salt. (footnote b) 1 mM 3-(4-nitrophenyl)pentanedioic acid instead of 1 mM NaAA was used. *Statistically significant ($P < 0.05$). (c) More hydrophobic degradation products were observed in the HPLC analyses. (d) General scheme of photolysis. (e) The peak of radical anion (SiPc-OR) was observed at 1 min $h\nu$ in Ar status (low-O_2 conditions) as seen in absorbance profiles. The radical anion disappeared once it contacted O_2.

space, ICD occurs as early as 1 min after treatment and results in irreversible morphologic changes on the target-expressing cell while sparing receptor-negative cells.[1,9,10] ICD induced by NIR-PIT rapidly maturates immature dendritic cells adjacent to dying cancer cells initiating a host anticancer immune response.[8] This is very different from photodynamic therapy that induces a combination of necrosis and apoptosis in both targeted cells and adjacent nontargeted cells and tends to create an inflammatory rather than an immunologic response.[11−14]

Additionally, loss of IR700-fluorescence that was a characteristic sign of successful NIR-PIT was observed with relatively low energy of light[15] despite the photostability and chemical stability of phthalocyanine cores. Therefore, we hypothesized that a unique photochemical reaction might be occurring, which is distinct from conventional reactive oxygen species production. In this paper, we investigate photochemical axial ligand-release reaction of IR700 when exposing NIR light, the effects to a covalently conjugated antibody, and the relationship to the biological effects to the conjugate-bound cells.

In this paper, we identify a photochemical axial ligand-releasing reaction of IR700 when exposed to NIR light, and the subsequent effects on an antibody to which the dye is covalently conjugated resulting in potential highly selective cytotoxic effects.

RESULTS

Photolysis of Pc 3 Produced Hydrophobic Degradation Products. For precise chemical analysis in photolysis, **Pc 3**, the phthalocyanine moiety of IR700, was synthesized, and the changes in chemical structure of the compound after NIR light irradiation were analyzed. The compounds were synthesized according to Figure 1a. **Pc 3** was precipitated by NIR light irradiation in the electron donor (NaAA) added condition but not in the electron acceptor added condition, and the absorbance of the solution was decreased (Figure. 1b). The phenomenon was independent of oxygenation conditions. In the HPLC analyses, more hydrophobic degradation products were observed with NaAA (Figure. 1c). The degradation product fraction was sampled, and the chemical structure of degradation product A was confirmed with MS and NMR. Degradation product B could not be analyzed with NMR because of insolubility; however, MS analysis matched with the molecular weight of degradation product B, and its HPLC retention time was concordant with the authentic compound. Consequently, we confirmed that axial ligands of **Pc 3** were cleaved with irradiation (Figure 1d).

Absorbance spectrum analysis revealed a peak at 577.5 nm which was present when the compound was exposed to NIR light in deoxygenated conditions but was not present in oxygenated conditions (Figure 1e). This peak represents the radical anion formed in this photolysis reaction and with oxygen acting as either a quencher of the triplet state or the radical anion. In total, the photolytic reaction involves radical anion production from the triplet excited state.[16]

NIR Light Causes Release of Axial Ligands Making IR700 Both Nonfluorescent and Hydrophobic. Next, we evaluated the photolysis of IR700 after NIR light irradiation. As in **Pc 3**, hydrophobic precipitation was observed after NIR light irradiation, and the molecules stopped fluorescing (Figure 2a). The fluorescence and absorbance were decreased in a

DOI: 10.1021/acscentsci.8b00565
ACS Cent. Sci. 2018, 4, 1559−1569

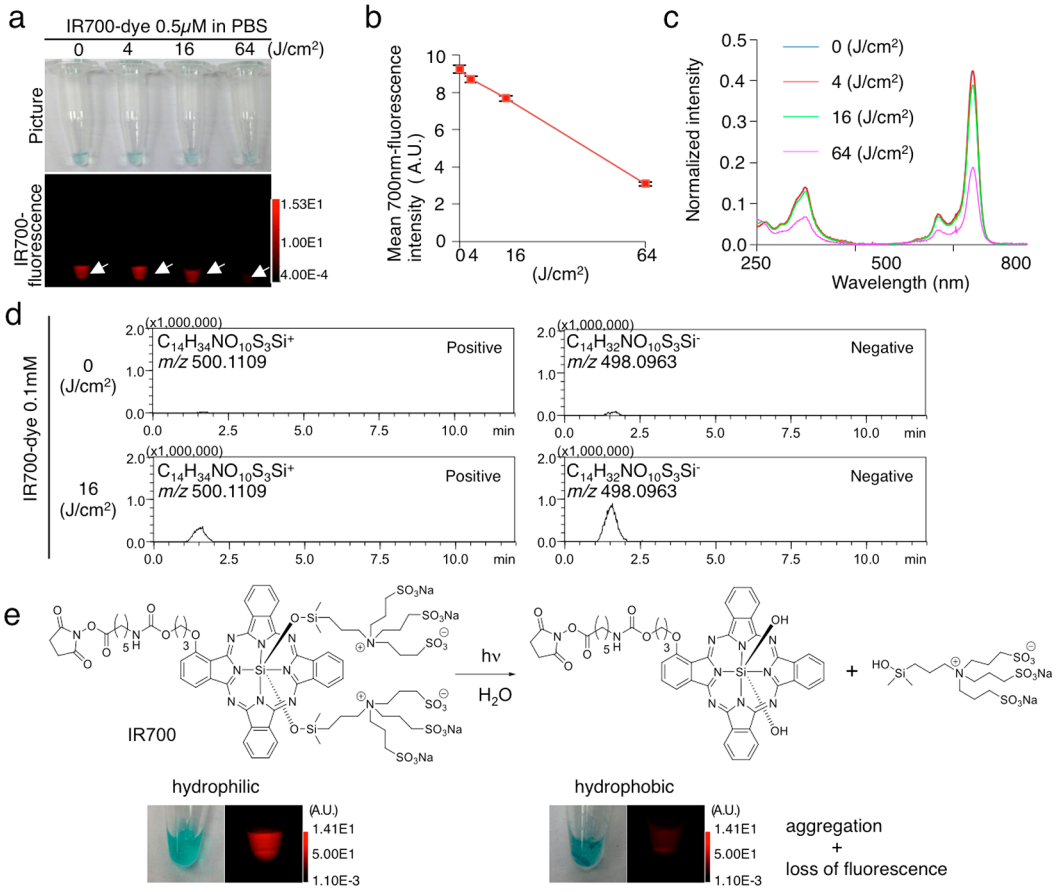

Figure 2. Releasing ligand with NIR light makes IR700DX-dye hydrophobic causing loss of its fluorescence. (a) 0.5 μM IR700-dye in PBS was irradiated with NIR light, and imaged in white light using a 700 nm filter. Both the blue color in the tube and the 700 nm fluorescence decreased in a light-dose-dependent manner. (b) Mean 700 nm fluorescence intensity was decreased in a dose-dependent manner (n = 3). (c) Absorbance profile showed decrease of the absorbance at the Q-band at 690 nm of the silicon phthalocyanines (SiPcs). (d) Mass spectroscopy detected released ligand ($C_{14}H_{34}NO_{10}S_3Si$) only in the NIR-light-irradiated (16 J cm^{-2}) tube (0.1 mM IR700-dye in PBS). With isotopic peak analysis, the peak was matched to the ligand ($C_{14}H_{34}NO_{10}S_3Si$) (Figure S1). (e) Hypothesized change of chemical structure of IR700-dye with NIR light irradiation. NIR light irradiation causes IR700-dye releasing the ligand ($C_{14}H_{34}NO_{10}S_3Si$), which makes IR700 hydrophobic and creates aggregation. Along with the change from hydrophilic to hydrophobic solubility, the blue color of IR700 decreases, and aggregation appears, while IR700-fluorescence is lost, as shown in part a.

light-dose-dependent manner (Figure 2a–c). In MS analysis, we detected the released axial ligand ($C_{14}H_{34}NO_{10}S_3Si$) from IR700 after NIR light irradiation (Figure 2d, Figure S1). This agrees with the observation in **Pc 3**, and confirms that NIR light causes ligand release, which makes IR700 hydrophobic leading to aggregation (Figure 2e).

A similar phenomenon was observed in mAb-IR700 conjugates, but it occurred at lower energy levels than the single dye molecule (Figure 3a–d, Figures S2a–c and S3a–c). The aggregates increased in size in a light-dose-dependent manner (Figure 3e, Figure S4). In SDS-PAGE analysis, we found that the irradiated antibody conjugate formed non-fluorescent aggregates that were larger than IgG, and fluorescence was quenched (Figure 3f, Figures S2d and S3d). Aggregation was also observed when the conjugate was bound to antigen (Figure 3g, Figure S2e). Thus, after NIR irradiation, mAb-IR700 becomes hydrophobic, aggregates, and loses fluorescence. Axial ligand release from mAb-IR700 conjugates was confirmed with a mass analysis (Figure 3h, Figure S5a–c).

Post-NIR Light Irradiation Protein Conformation Changes in mAb-IR700 Are Detected by AFM. The conformational change of the mAb-IR700 conjugate after NIR light irradiation was observed with FM-AFM. Prior to NIR light irradiation the conjugates were spread homogeneously on mica. After NIR light irradiation, each conjugate became enlarged, and the number of conjugates attached to the mica increased (Figure 4a). The single-molecule AFM showed that NIR light irradiation resulted in enlargement with loss of the normal Y-shape of the antibody (Figure 4b). Three independent experiments showed increases in both height and area of the conjugate after NIR irradiation, and aggregates could be seen on the mica plate (Figure 4c). These data suggested that NIR light induced changes in the conformation of the mAb-IR700 conjugate, and dimers or oligomers of the conjugates were formed.

NIR-Light-Induced Photochemical Changes Predicted Cell Death in Vitro. To evaluate the relationship between the axial ligand release due to photochemical reaction and NIR-PIT targeted cell death in vitro, we studied the loss of IR700-fluorescence with respect to cell killing. As shown, NIR light leads to ligand release and increases in hydrophobicity of silicon phthalocyanine. A431-luc-GFP cells pretreated with pan-IR700 and exposed to NIR light irradiation showed reduced IR700-fluorescence due to photolysis. GFP-fluorescence also decreased but for different reasons: the dye escaped from the cell after NIR-PIT caused cell rupture (Figure S6a).

DOI: 10.1021/acscentsci.8b00565
ACS Cent. Sci. 2018, 4, 1559–1569

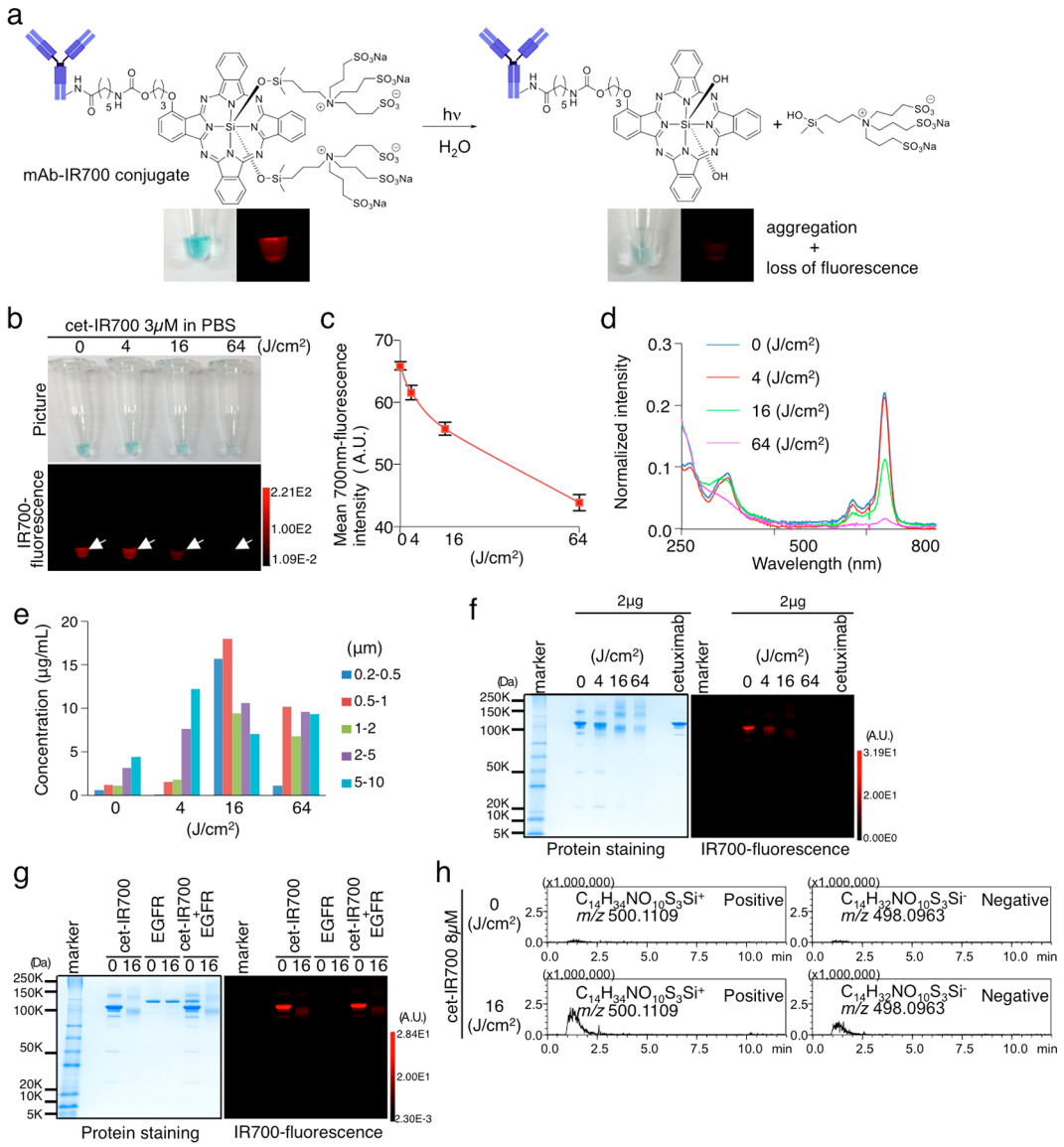

Figure 3. Releasing ligand with NIR light makes mAb-IR700 conjugates hydrophobic causing aggregation and loss of fluorescence. (a) Hypothesized change of chemical structure of mAb-IR700 with NIR light irradiation. NIR light irradiation causes mAb-IR700 to release the ligand ($C_{14}H_{34}NO_{10}S_3Si$), which makes mAb-IR700 hydrophobic and causes aggregation. Along with the change from hydrophilic to hydrophobic, the blue color of mAb-IR700 conjugate decreases; aggregation appears, and IR700-fluorescence is lost. (b) 3 μM cet-IR700 in PBS was irradiated with NIR light, and imaged in white light and 700 nm fluorescence. Both the blue color in the tube and the 700 nm fluorescence decreased in a light-dose-dependent manner. (c) Mean 700 nm fluorescence intensity of cet-IR700 in PBS was decreased in a dose-dependent manner (n = 3). (d) Absorbance profile of cet-IR700 in PBS with NIR light irradiation measured showed decrease of the absorbance at the Q-band at 690 nm of the SiPcs. (e) Analysis of aggregated particles with an aggregate-sizer was examined at increasing NIR light irradiation 4, 16, and 64 J cm^{-2}. (f) SDS-PAGE of NIR-light-irradiated cet-IR700 revealed that the protein band of cetuximab disappeared in a dose-dependent manner, and some bands over cetuximab increased with smear. The IR700-fluorecence in the SDS-PAGE decreased in a light-dose-dependent manner. (g) The complex of cet-IR700 and recombinant EGFR protein was irradiated with NIR light and electrophoresed by SDS-PAGE. The protein bands of not only cet-IR700 but also EGFR become thin with a smear over its protein band along with loss of IR700-fluorescence. (h) IT-TOF-MS detected release of the ligand ($C_{14}H_{34}NO_{10}S_3Si$) from cet-IR700 after NIR light irradiation (16 J cm^{-2}). With analysis of the isotope peak and product ion scan, the peak was confirmed as the ligand ($C_{14}H_{34}NO_{10}S_3Si$) (Figure S3).

We evaluated A431-luc-GFP cell viability with luciferase imaging in vitro. Cell viability (i.e., bioluminescence signal) decreased in a light-dose-dependent manner (Figure S6b). The reduced IR700-fluorescence of pan-IR700 in treated cells was measured by flow cytometry, using MFI (mean fluorescence intensity). The fluorescence of pan-IR700 decreased in a light-dose-dependent manner (Figure S6c). A positive correlation (r = 0.977 79, p < 0.0001) was observed between decreased bioluminescence and IR700-fluorescence (Figure S6d). We also tested the A431-luc-GFP cell with cet-IR700, MDAMB468-luc-GFP cell with pan-IR700 or cet-IR700, 3T3/Her2-luc-GFP cell with tra-IR700, and Calu3-luc-GFP cell with tra-IR700, and observed the same positive correlation between loss of bioluminescence and IR700-fluorescence (Figures S7–S11a–d). These data supported the hypothesis that ligand release of IR700 is linked to cell death after NIR-PIT.

DOI: 10.1021/acscentsci.8b00565
ACS Cent. Sci. 2018, 4, 1559–1569

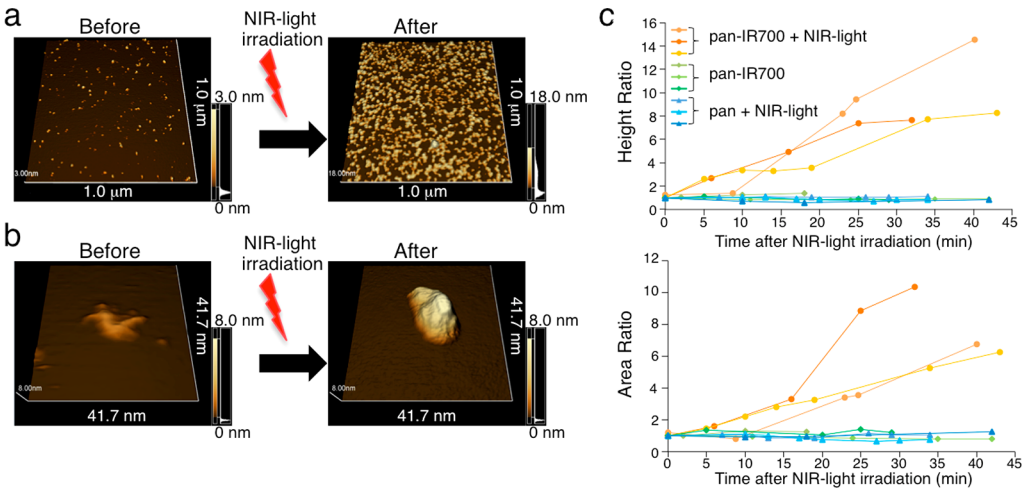

Figure 4. Single-molecule imaging of the change of mAb-IR700 conjugates after NIR light irradiation. (a) 1.0 μm^2 view of pan-IR700 on the mica was imaged with FM-AFM. After NIR light irradiation, more pan-IR700 is attached to the mica, and the size of pan-IR700 increases (4 J cm^{-2}). (b) Single molecule of pan-IR700 on mica changes in volume and shape after NIR light irradiation. (c) Quantitative analysis of height and area of the particles on mica demonstrates that NIR-light-irradiated (4 J cm^{-2}) pan-IR700 results in larger and longer molecules. Only pan-IR700 or irradiated panitumumab (pan) showed no change in the height and area (n = 3 to each group).

Changes in the Chemical Characteristics of IR700 Lead to Targeted Cell Death in Vivo. Next, we tested whether the reduced IR700-fluorescence correlates with the antitumor effect in vivo using a xenograft tumor model. The therapeutic regimen is shown (Figure 5a). We evaluated bioluminescence of three tumors in the same mouse, and each tumor was irradiated with either 0 (control), 10, or 50 J cm^{-2} NIR light, respectively (Figure 5b). We measured the IR700-fluorescence and bioluminescence in each tumor before and after the NIR light irradiation (Figure 5c). A positive correlation (r = 0.6316, p < 0.0001) was observed between loss of bioluminescence and IR700-fluorescence in the tumors (Figure 5d). We also evaluated the A431-luc-GFP tumor with cet-IR700, MDAMB468-luc-GFP tumor with pan-IR700 or cet-IR700, 3T3/Her2-luc-GFP tumor with tra-IR700, and Calu3-luc-GFP tumor with tra-IR700, and also observed the same correlation. (Figures S7−S11e,f). These data support the hypothesis that axial ligand release of IR700 after NIR light irradiation leads to the cell death.

For a further evaluation of the chemical structural change of IR700, biodistribution studies of ^{111}In-DTPA-labeled pan-IR700 (^{111}In-DTPA-pan-IR700) were conducted with and without NIR light irradiation to the abdomen, after intravenous injection of ^{111}In-DTPA-pan-IR700. ^{111}In-DTPA-pan-IR700 with NIR light irradiation quickly led to accumulation of the tracer in the liver and spleen, which was quickly cleared from the blood, with less accumulation in the tumor compared to nonirradiated conjugate (Figure 5e). These results indicate that NIR light irradiation caused aggregates to form that were recognized by the reticuloendothelial system (RES).

Released Ligand Quickly Excreted into the Urine after NIR-PIT in Vivo. For a demonstration of the ligand release from antibody-IR700 conjugates by exposing NIR light irradiation in vivo, semiquantitative LC/MS/MS analysis of the ligand in urine obtained from MDAMB468-luc-GFP tumor-bearing mice was performed before and after NIR-PIT (Figure 5f). Fluorescence of pan-IR700 in the tumor immediately decreased after exposure of NIR light (Figure 5g). No ligand was detected before pan-IR700 injection (−24 h). The small amount of ligand was detected from all urine samples collected even before NIR-PIT (0 h) (Figure 5h). The ligand amount in urine of the NIR-PIT-treated mice drastically increased 1 and 2 h after NIR-PIT, and then quickly decreased afterward. On the other hand, the ligand amount in urine of no NIR light exposure mice was almost unchanged. There were significant differences of ligand amount in urine between the groups at 2 and 3 h after NIR light exposure (p < 0.05). These data suggested that the ligands were released from antibody-IR700 conjugates after exposure to NIR light, and then were quickly excreted into the urine within a few hours.

DISCUSSION

When IR700 is exposed to NIR light, both axial ligands attached to the silicon atom at the core of phthalocyanine dissociate with hydrolysis especially under electron-donor-rich conditions (Figure 1d). After dissociation, the phthalocyanine core precipitated in aqueous solution indicating a transition from a highly hydrophilic molecule to one that is much less soluble (Figure 2e). During this reaction, an intermediate anion radical is observed (Figure 1e).[16] The radical anion is produced preferably in hypoxic conditions from the triplet excited state.[16]

When IR700 was conjugated with an antibody molecule, ligand dissociation from IR700 affected the shape and solubility of the antibody to which it is attached as well as antibody−antigen complexes (Figure 3a). When antibody-IR700 conjugates in aqueous solution are exposed to relatively low levels of NIR light, antibody molecules could be observed to change shape and aggregate using FM-AFM which was confirmed with aggregate-sizers, and gel-electrophoresis under electron-donor-poor conditions (Figures 3 and 4). Additionally, if the antibody conjugate was bound to its cognate antigen, similar changes were observed (Figure 3g). Following this reaction, NIR-fluorescence was lost, and IR700 could not reach the triplet state;[17] therefore, we hypothesize that no further photochemical reaction is possible at this point.

Decreased IR700-fluorescence correlated with cytotoxicity in target cells in vitro and target tumors in vivo (Figure S6d, Figure 5d); therefore, these results suggested that the axial ligand-release reaction of IR700 leads to profound physical

DOI: 10.1021/acscentsci.8b00565
ACS Cent. Sci. 2018, 4, 1559−1569

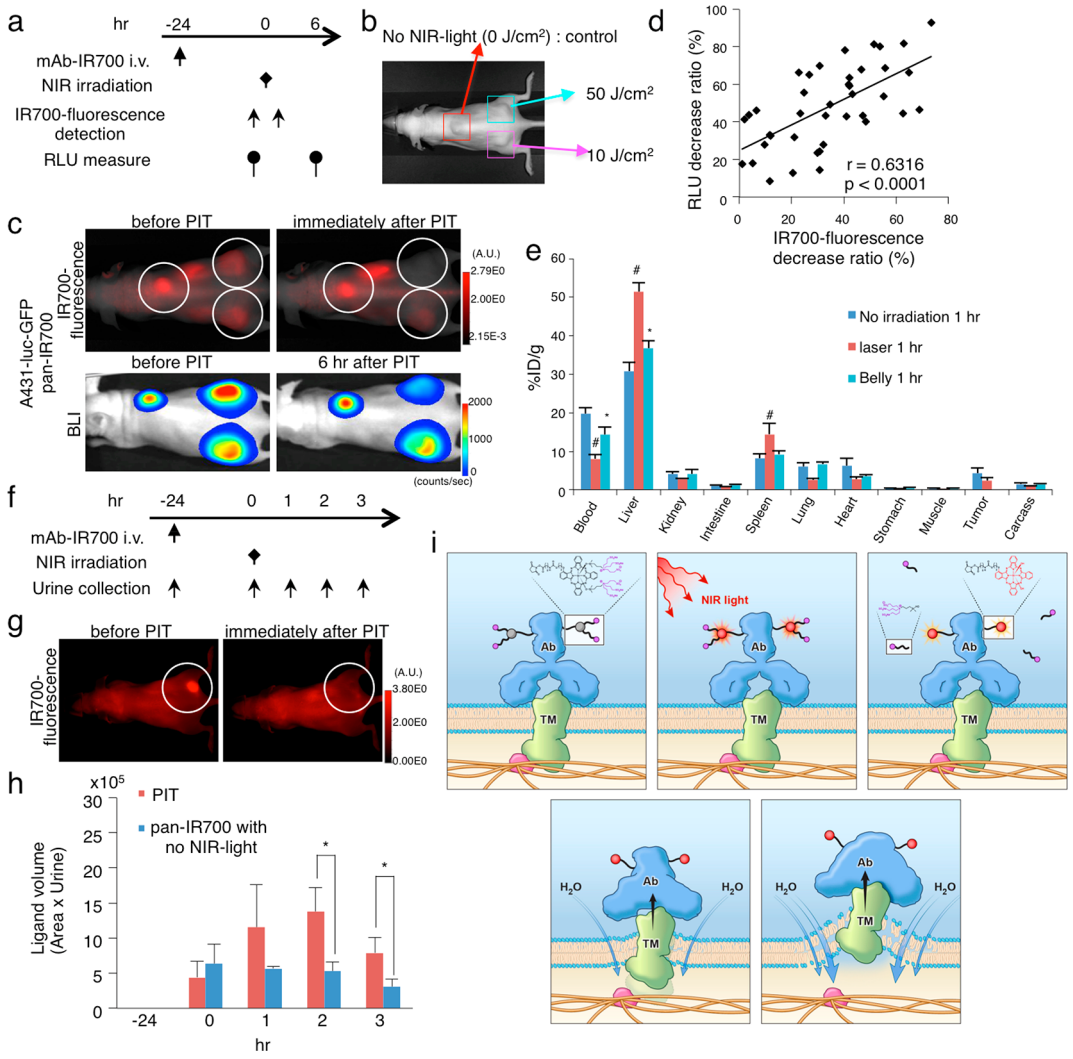

Figure 5. NIR-PIT antitumor effect in vivo was detected as the loss of IR700-fluorescence while the released ligand was quickly excreted into the urine after NIR-PIT in vivo. Scheme indicates the proposed mechanism of NIR-PIT. (a) The regimen of NIR-PIT is shown. Images were obtained at each time point as indicated. (b) Triple subcutaneous tumor model was prepared as pictured, and each tumor was irradiated as indicated. (c) In vivo BLI and IR700-fluorescence imaging of subcutaneous tumor model before and at 6 h after the NIR light irradiation. (d) A positive correlation was detected between RLU decrease ratio and IR700-fluorescence decrease ratio (n = 40, r = 0.6316, p < 0.0001, Peason's product moment correlation coefficient). (e) In vivo biodistribution of ^{111}In-DTPA-IR700-panitumumab radioactivity at 1 h after injection ^{111}In-DTPA-IR700-panitumumab (control), NIR-light-irradiated (16 J cm^{-2}) ^{111}In-DTPA-IR700-panitumumab, or NIR light irradiation to the mice belly (16 J cm^{-2}) after injection of ^{111}In-DTPA-IR700-panitumumab were examined. NIR-light-irradiated (16 J cm^{-2}) ^{111}In-DTPA-IR700-panitumumab or NIR light irradiation for mice belly (16 J cm^{-2}) resulted in increases in liver and spleen activity compared to control (n = 5 mice in each group; *p < 0.05, #p < 0.01). (f) The regimen of NIR-PIT is shown. Mice urine samples were obtained at each time point as indicated. (g) NIR light exposure immediately decreased IR700-fluorescence intensity in tumors. White circle indicate tumor beds. (h) The released ligand in the urine was semiquantitatively evaluated by LC/MS/MS analysis. The ligand quickly increased after NIR-PIT, showing significant difference 2 and 3 h after NIR light exposure (n = 3, *p < 0.05). The ligand in urine of the no NIR-PIT group slightly decreased over time. No ligand was detected in the urine before pan-IR700 injection. (i) Scheme indicates the proposed mechanism of NIR-PIT. An antibody-IR700-antigen complex is formed on the cell membrane. With NIR light irradiation, the ligands of IR700 were released form the antibody-IR700-antigen complex. The physical changes in aggregation and solubility of the antibody-IR700-antigen complex may produce physical stress on the membrane locally impairing cellular membrane function for maintaining membrane pressure, and then the water outside of the cell was flown into the cell to burst the cell.

changes within the antibody-IR700-antigen complex which in turn could cause cell membrane damage to target cells. Released ligands were rapidly excreted into the urine within several hours after exposing NIR light for NIR-PIT in vivo (Figure 5h) which could reflect numbers of reacted molecules with this photoinduced ligand-release reaction. When this reaction occurs at the cellular membrane, physical changes in aggregation and solubility may produce physical stress on the membrane locally impairing cellular membrane function for maintaining membrane pressure (Figure 5i). Accumulation of such events on the cellular membrane could induce weakness in the membrane integrity leading to the swelling, blebbing, and bursting associated with photoimmunotherapy. Our previous finding that hypoxic conditions did not compromise the cytotoxicity[18] supports ligand release hypothesis.

There are currently limitations in microscopic technology that can visualize such local molecular changes on living cells which make it difficult to prove that this reaction is responsible for the cytotoxicity induced by NIR-PIT. As shown in Videos S1−S3, in the Supporting Information, taken with two recently

DOI: 10.1021/acscentsci.8b00565
ACS Cent. Sci. 2018, 4, 1559−1569

developed high-resolution live cell microscopes, a quantitative phase microscope (QPM) and dual-angle selective plane illumination microscope (diSPIM), morphological changes of NIR-PIT treated cells within minutes (Videos S1−S3) which coincides with the reaction kinetics of IR700 dissociation. To actually visualize such changes on the cellular membrane would require resolution of less than 100 nm at a temporal resolution of less than 10 s. Therefore, with current technology it is difficult to observe physical changes on the cellular membrane and visualize the physicochemical changes observed in vitro.

In conclusion, the photoinduced axial ligand-releasing reaction on a silicon phthalocyanine derivative (IR700) is induced with relatively low-energy NIR light. When a silicon phthalocyanine derivative is conjugated to an antibody and exposed to NIR light, the reaction greatly affected the shape and induced dimerization or aggregation of the conjugate or conjugate-antigen complex in aqueous solution. When this reaction occurred in antibody-IR700 conjugates bound to cell membrane proteins, it is plausible that the photoinduced reaction caused stress in the cellular membrane impairing its function, and resulting in killing of cells consistent with the observed clinical and preclinical effects of NIR-PIT.

MATERIALS AND METHODS

Study Design. Our primary research objective was to elucidate the mechanism of NIR-PIT. The overall study design was a series of controlled laboratory experiments as indicated in the sections below. Animal models were evaluated with in vivo imaging such as luciferase activity. All in vivo procedures were conducted in compliance with the Guide for the Care and Use of Laboratory Animal Resources (1996) and US National Research Council, and they were approved by the NIH Animal Care and Use Committee.

Reagents. Water-soluble, silicon phthalocyanine derivative, IRDye700DX NHS ester (IR700), was obtained from LI-COR Bioscience (Lincoln, NE). Panitumumab, a fully humanized IgG_2 mAb directed against EGFR, was purchased from Amgen (Thousand Oaks, CA). Trastuzumab, 95% humanized IgG_1 mAb directed against HER2, was purchased from Genentech (South San Francisco, CA). Cetuximab, a chimeric (mouse/human) mAb directed against EGFR, was purchased from Bristol-Meyers Squibb Co (Princeton, NJ). All other chemicals were of reagent grade.

Synthesis of Phthalocyanine Moiety of IR700 for Structural Analysis after Photolysis. The compounds were synthesized according to Figure 1a. ^{1}H NMR spectra were recorded on a JNM-ECX400P or JMN-ECS400 (JEOL Ltd., Tokyo, Japan) instrument at 400 MHz and are reported relative to deuterated solvent signals (Figures S12−S15). ESI and MALDI-TOF mass spectra were recorded on a JMS-T100LP (JEOL Ltd.) or an Ultraflex II TOF/TOF (Bruker Japan K.K., Kanagawa, Japan) instrument, respectively.

*Silicon Phthalocyanine Dihydroxide (**Pc 1**).* The compound was prepared by a modification of the synthesis reported by Davison and Wynne.[19] Silicon tetrachloride (300 mg, 1.77 mmol) and 1,3-diiminoisoindoline (176 mg, 1.21 mmol) were dissolved in quinoline (2 mL), and the mixture was refluxed for 2 h under an Ar atmosphere. After the mixture was cooled to room temperature, 1 M NaOH aq (2 mL) was added, and the mixture was refluxed for 1 h. The product (111 mg, 0.194 mmol) was recovered by filtration, washed with MeOH, and dried in vacuo. MS (MALDI$^+$) m/z: $[M + H]^+$ calcd for $C_{32}H_{19}N_8O_2Si$, 575.1; found, 574.7.

*Bis(3-aminopropyldimethylsilyl oxide) Silicon Phthalocyanine (**Pc 2**).* The compound was prepared by a modification of previously reported method.[20] **Pc 1** (50 mg, 0.087 mmol) and 3-aminopropyldimethylethoxysilane (140 mg, 0.87 mmol) were dissolved in pyridine (40 mL), and the mixture was refluxed for 6 h under an Ar atmosphere, concentrated by rotary evaporation (<35 °C). The residue was diluted, filtered, washed with a H_2O−ethanol solution (2:1), and dried in vacuo (47 mg, 0.0583 mmol, yield 43% (3 steps)). ^{1}H NMR (400 MHz, $CDCl_3$): δ −2.86 (s, 12H), −2.34 to −2.27 (m, 4H), −1.28 to −1.19 (m, 4H), 1.18 (t, J = 7.2 Hz, 4H), 8.35 (dd, J = 5.7, 2.9 Hz, 8H), 9.65 (dd, J = 5.7, 2.9 Hz, 8H). HRMS (ESI$^+$) m/z: $[M + Na]^+$ calcd for $C_{42}H_{45}N_{10}O_2Si_3Na$, 827.2849; found, 827.2848.

*Bis{3-[tris(3-sulfopropyl)]ammoniopropyldimethylsilyl oxide} Silicon Phthalocyanine (**Pc 3**).* **Pc 2** (40 mg, 0.050 mmol), 1,3-propansultone (72.8 mg, 0.60 mmol), and *N*,*N*-diisopropylethylamine (DIEA, 84.7 mg, 0.66 mmol) were dissolved in MeOH (2 mL), and the mixture was stirred at 50 °C for 48 h under an Ar atmosphere. The product was purified by an HPLC system (Shimadzu Co., Kyoto, Japan) with a reverse-phase column Inertsil ODS-3 (10 mm × 250 mm) (GL Sciences Inc., Tokyo, Japan), using eluent A (H_2O, 0.1 M triethylammonium acetate (TEAA)) and eluent B (99% MeCN, 1% H_2O) (A/B = 80/20 to 50/50 in 15 min, 50/50 to 0/100 in 5 min). The product was desalted with a Sep-Pak C18 cartridge (Waters Corporation, Milford, MA) and cation-exchange resin, affording **Pc 3** (16.3 mg, 0.010 mmol, yield 20% as a sodium salt). ^{1}H NMR (400 MHz, CD_3OH): δ −2.79 (s, 12H), −2.15 (t, J = 8.1 Hz, 4H), −0.87 to −0.97 (m, 4H), 1.76−1.66 (m, 12H), 2.02 (t, J = 8.1 Hz, 4H), 2.81−2.72 (m, 24H 8.55−8.49 (m, 8H), 9.82−9.76 (m, 8H)). HRMS (ESI$^+$) m/z: $[M + Na]^+$ calcd for $C_{60}H_{76}N_{10}Na_5O_{20}S_6Si_3$, 1647.2358; found, 1647.2358.

Structural Analyses of Silicone Phthalocyanine (Pc 3) after Photolysis. For Figure 1b, a solution of **Pc 3** (1 μM) in PBS buffer (pH 7.5) with 1 mM L-ascorbic acid sodium salt (NaAA) for an electron donor or 1 mM 3-(4-nitrophenyl)-pentanedioic acid for an electron acceptor was prepared in a quartz cuvette, and the absorption spectrum was measured with a UV spectrophotometer UV-1800 (Shimadzu Co.). Then, the solution was irradiated with excitation light of a spectrofluorometer FP-8600 (JASCO Corporation, Tokyo, Japan) (676.5 nm, 3.5 mW cm^{-2}) for 30 min, and the absorption spectrum was measured again. The percentage of decrease in absorbance (676.5 nm) after irradiation was calculated. The deoxygenated solutions were prepared by bubbling Ar through the septum cap of the sealed cuvette. The experiments were conducted in triplicate. For Figure 1e, a solution of **Pc 3** (1 μM) in deoxygenated PBS buffer (pH 7.5) with 1 mM L-cysteine hydrochloride was prepared in the sealed quartz cuvette, and the absorption spectra were measured. Then, the solution was irradiated by a laser MLL-III-690 (Changchun New Industries Optoelectronics Technology Co. Ltd., Changchun, China) (690 nm, 20 mW cm^{-2}) for 1 min, and the absorption spectrum was measured. Then, the sealed cuvette was opened for aeration, and the absorption spectrum was measured. The power densities were measured with an optical power meter PM200 (Thorlabs, Inc., Newton, NJ). All the experiments were carried out at room temperature.

DOI: 10.1021/acscentsci.8b00565
ACS Cent. Sci. 2018, 4, 1559−1569

Characterization of Photolysis. A 1 μM solution of **Pc 3** in PBS buffer (pH 7.5) with 1 mM NaAA was irradiated with excitation light of a spectrofluorometer FP-8600 (676.5 nm, 3.5 mW cm^{-2}) for 30 or 60 min. HPLC analyses of the photolysis were performed by an HPLC system (Shimadzu Corporation) with a reverse-phase column Inertsil ODS-3 (4.6 mm × 250 mm) (GL Sciences Inc.), using eluent A (H_2O, 0.1 M TEAA) and eluent B (99% MeCN, 1% H_2O) (A/B = 80/20 to 0/100 in 10 min; flow rate, 1.0 mL min^{-1}). The products by photolysis were isolated and characterized with NMR and MS (ESI and MALDI-TOF).

Degradate A. ^{1}H NMR (400 MHz, DMSO-d_6): δ −2.93 (s, 6H), −2.48 (s, 1H), −2.41 to −2.35 (m, 2H), −1.07 to −0.95 (m, 2H), 1.37−1.48 (m, 6H), 1.83−1.91 (m, 2H), 2.25−2.34 (m, 12H), 8.47 (dd, 8H, J = 5.6, 3.1 Hz), 9.69 (dd, 8H, J = 5.6, 3.1 Hz). MS (ESI^+) m/z: $[M+TEA]^+$ as TEA salt, calcd for $C_{52}H_{63}N_{10}Na_2O_{11}S_3Si_2$, 1201.3; found, 1201.3.

Degradate B. MS ($MALDI^+$) m/z: $[M + H]^+$ calcd for $C_{32}H_{19}N_8O_2Si$, 575.1; found, 574.7.

Conjugation of IR700-Conjugated Trastuzumab, Panitumumab, or Cetuximab. Conjugation of IR700 with mAbs was performed according to previous reports.[21−23] In brief, panitumumab, trastuzumab, or cetuximab (1 mg, 6.8 nmol) was incubated with IR700 NHS ester (60.2 μg, 30.8 nmol) in 0.1 mol L^{-1} Na_2HPO_4 (pH 8.6) at room temperature for 1 h. The mixture was purified with a Sephadex G25 column (PD-10; GE Healthcare, Piscataway, NJ). The protein concentration was determined with the Coomassie Plus protein assay kit (Thermo Fisher Scientific Inc., Rockford, IL) by measuring the absorption at 595 nm (8453 Value System; Agilent Technologies, Santa Clara, CA). The concentration of IR700 was measured by absorption at 689 nm to confirm the number of IR700 molecules conjugated to each mAb. The synthesis was controlled so that an average of three IR700 molecules were bound to a single antibody. We performed SDS-PAGE as a quality control for each conjugate.[21] We abbreviate panitumumab-IR700 as pan-IR700, cetuximab-IR700 as cet-IR700, and trastuzumab-IR700 as tra-IR700.

Detection of Release of the Axial Ligand ($C_{14}H_{34}NO_{10}S_3Si$). A 50 μL portion, in tube, of 0.1 mM IR700 in PBS containing 5 mM L-cystein as an electron donor was irradiated with NIR light (16 J cm^{-2}) or was not prepared, and supernatant was examined. A 50 μL portion, in tube, of 8 μM cet-IR700 in PBS containing 5 mM L-cystein was also irradiated with NIR light (16 J cm^{-2}) or was not prepared, and supernatant was tested as follows. MS^n analysis with high mass accuracy was performed on an ultra-high-performance chromatograph (Nexera X2 UHPLC system, Shimadzu Co.) coupled to a hybrid ion-trap time-of-flight mass spectrometer (LCMS-IT-TOF, Shimadzu Co.). The mobile phase consisted of 0.1% (v/v) formic acid in water (A) and 0.1% (v/v) formic acid in acetonitrile (B), and was delivered at a flow rate of 0.2 mL min^{-1}. The following gradient conditions were used: 2% B (0.0 min), 60% B (10.0 min), 98% B (10.1−14.0 min), 2% B (14.1 min), and STOP (19.0 min). A Kinetex C18 column (2.1 mm i.d. × 50 mm L, 5 μm, Phenomenex) was used as analytical column. The column oven temperature was set at 40 °C. The LCMS-IT-TOF parameters were set as follows: ESI with positive and negative switching mode, probe voltage of +4.5/−3.5 kV, nebulizing gas flow rate of 1.5 L min^{-1}, drying gas pressure of 0.1 MPa, CDL temperature of 200 °C, and block heater temperature of 200 °C. The mass range was set at m/z 100−1000 for MS^{1-3} analyses. The ion accumulation time was set at 10 or 30 ms for MS^1 or MS^{2-3} analyses, respectively. The precursor ions for MS^2 or MS^3 analysis were selected automatically, triggered by peak intensity information in the MS^1 or MS^2 spectrum, respectively.

A Nexera X2 UHPLC system coupled to a triple quadrupole mass spectrometer (LCMS-8050, Shimadzu Co.) was used for semiquantitative analysis of the axial ligand in the urine sample. The mobile phase consisted of 20 mM ammonium formate in water (A) and acetonitrile (B), and was delivered at a flow rate of 0.4 mL min^{-1}. The gradient condition was set as 1% B (0.0 min), 40% B (5.0 min), 98% B (5.1−7.0 min), 1% B (7.1 min), and STOP (10 min). Injection volume was 1 μL. Chromatographic separation was achieved on a Scherzo SM-C18 column (2.0 mm i.d. × 150 mm L, 3 μm, Imtakt). The column oven temperature was set at 40 °C. The LCMS-8050 parameters were set as follows: ESI positive mode, probe voltage of +4.0 kV, nebulizing gas flow rate of 2.0 L min^{-1}, drying gas flow of 10 L min^{-1}, heating gas flow of 10 L min^{-1}, DL temperature of 250 °C, and block heater temperature of 400 °C. The MRM transitions were of 500.00 > 75.10, 500.00 > 458.00, 500.00 > 440.00, and 500.00 > 197.00.

Fluorescence Evaluation of IR700-Dye or mAb-IR700 in Vitro. The IR700-fluorescence intensity was acquired with a fluorescence imager (Pearl Imager, LI-COR Bioscience). The same ROI was put on the solution in each tube, and mean IR700-fluorescence was measured. The IR700-fluorescence was also examined by spectroscopy (8453 Value System). The appearance of the tube before and after NIR light irradiation was imaged.

Evaluation of mAb-IR700 Aggregation with NIR Light Irradiation. SDS-PAGE was done after irradiation of NIR light for mAb-IR700. IR700-fluorescence was imaged with a PEARL imager. EGFR recombinant protein was commercially obtained (ORIGENE, MD). EGFR and cat-IR700 or pan-IR700 was mixed and incubated for 1 h, then washed with PBS twice, and then irradiated with NIR light. The sizes of aggregates were measured with an aggregate-sizer (Aggregates Sizer, Shimadzu Co.). The condition on analysis was 1.41−0.10 in refractive index, 1.37 g mL^{-1} in density.

Single-Molecule Imaging of mAb-IR700. Single-molecule FM-AFM (atomic-force microscope) imaging was performed according to a previous report.[24] The 2 μg mL^{-1} pan-IR700 or panitumumab was placed on the mica disc in 10 mM phosphate buffer containing 50 mM $MgCl_2$. A scanning probe microscope (FM-AFM, SPM-8100FM, Shimadzu Co.) was modified so that the wavelength of the scan laser was 405 nm (usually 655 nm), which has less effect on the excitation of IR700. The image was taken before and after the NIR light irradiation. The statistical analysis was done with the software for the particle analysis.

Cell Culture. Luciferase- and GFP-expressing A431, MDAMB468, 3T3/Her2, and Calu3 cell lines were established by transducing them with RediFect Red-FLuc-GFP lentiviral particles (PerkinElmer, Waltham, MA).[9,10,22,23] Their high luciferase expression was confirmed through 10 passages. Cells were cultured in RPMI 1640 medium (Thermo Fisher Scientific Inc.) supplemented with 10% fetal bovine serum and 100 IU mL^{-1} penicillin/100 μg mL^{-1} streptomycin (Thermo Fisher Scientific Inc.).

In Vitro NIR-PIT. In 24-well plates, 100 000 cells were seeded and incubated with each of the following cell line and mAb-IR700 conjugate pairs (A431-luc-GFP, MDAMB468-luc-

DOI: 10.1021/acscentsci.8b00565
ACS Cent. Sci. 2018, 4, 1559−1569

GFP: pan-IR700 or cet-IR700; 3T3/Her2-luc-GFP, Calu3-luc-GFP: tra-IR700) at 10 μg mL^{-1} for 6 h at 37 °C. After the cells were washed with PBS twice, PBS was added. Then, cells were irradiated with either a red LED (L690-66-60; Marubeni America Co., Santa Clara, CA) or laser (BWF5-690-8-600-0.37; B&W TEK INC., Newark, DE). The power density was measured with an optical power meter (PM 100, Thorlabs, Newton, NJ) to emit the same light dose (J cm^{-2}) with either LED or laser, while the time of exposure was carefully adjusted.

Fluorescence Microscopy. On a glass-bottomed dish, 10 000 cells were seeded and incubated with each mAb-IR700 at 10 μg mL^{-1} for 6 h and washed twice with PBS, and PI was added at 2 μg mL^{-1} for 30 min. The cells were then exposed to near-infrared (NIR) light (4 J cm^{-2}), and images were obtained using a fluorescence microscope (IX61; Olympus America) with a filter set for IR700-fluorescence (590−650 nm excitation filter; 665−740 nm band-pass emission filter), GFP-fluorescence (457−487 nm excitation filter; 502−538 nm band-pass emission filter), and PI-fluorescence (542−582 nm excitation filter; 604−644 nm band-pass emission filter), respectively.

Flow Cytometry. Fluorescence from cells before and after NIR-PIT was measured using a flow cytometer (FACS Calibur, BD BioSciences, San Jose, CA) and CellQuest software (BD BioSciences). Cells (1×10^5) were incubated with each conjugate for 6 h at 37 °C, and then, NIR-PIT was performed. The decrease of IR700-fluorescence on the cells, was evaluated with MFI (mean fluorescence intensity) with or without NIR light irradiation. For validation of the specific binding of the conjugated antibody, excess antibody (50 μg) was used to block 0.5 μg of dye-antibody conjugates and confirmed the specificity.

Animals and Tumor Models. Six-to-eight-week-old female homozygote athymic nude mice were purchased from Charles River (NCI-Frederick). During all pain-inducing procedures, mice were anesthetized with isoflurane.

Four million A431-luc-GFP cells, two million 3T3/Her2-luc-GFP cells, six million MDAMB468-luc-GFP cells, or eight million Calu3-luc-GFP cells were injected subcutaneously in three positions of the mice, one as a control tumor (no NIR light irradiation); the left dorsal tumor was exposed to 10 J cm^{-2} irradiation, and the left dorsal tumor was exposed to 50 J cm^{-2} irradiation, respectively (Figure 5b). Mice with tumors measuring approximately 300 mm^3 (8−9 mm in the diameter) were used for the experiments. Mice were monitored daily, and when the tumor diameter reached 2 cm, the mice were euthanized with carbon dioxide.

In Vivo NIR-PIT. All mice were anesthetized with inhaled 3%−5% isoflurane immediately before NIR-PIT, and accumulation of pan-IR700 on the tumor beds was confirmed by a Pearl imager. Mice were intravenously injected 1 day before NIR light irradiation. NIR light via a laser (B&W TEK Inc.) was administered to tumors (except control), and the remainder of the mouse was covered with aluminum foil.

In Vivo Bioluminescence Imaging IR700-Fluorescence Imaging. For bioluminescence imaging (BLI), D-luciferin (15 mg mL^{-1}, 200 μL) was injected intraperitoneally, and the mice were imaged on a BLI system (Photon Imager; Biospace Lab, Nesles la Vallee, France). Regions of interest were set on the entire tumors to quantify the luciferase activity. IR700-fluorescence images before and after therapy were acquired with a fluorescence imager (Pearl Imager).

Biodistribution Study. A431-luc-GFP tumor-bearing mice were divided into four groups (n = 5) for biodistribution studies as described previously.[21] In brief, ^{111}In-DTPA-pan-IR700 was purified with a PD-10 size exclusion column. ^{111}In-DTPA-pan-IR700 (37 kBq/5 μg/100 μL in PBS/mouse) (normal) or ^{111}In-DTPA-pan-IR700 irradiated with 16 J cm^{-2} NIR light (laser) was injected via tail vein. After injection of ^{111}In-DTPA-pan-IR700, additional three mice were irradiated with 16 J cm^{-2} NIR light via the belly (Belly). Then the biodistribution was determined at 1 and 24 h postinjection by harvesting the organs, weighing them, and counting radioactivity using a 2480 automatic γ counter: Wizard^{2}3″ (PerkinElmer), with the remaining injected dose as a standard. The data are shown as the percentage injected dose per gram of tissue (%ID g^{-1}).

Detection of Released Ligand in the Urine after NIR-PIT in Vivo. The MDAMB468-luc-GFP xenografted mice were divided into two groups: (1) 100 μg of pan-IR700 i.v., no NIR light (Agent, n = 3); and (2) 100 μg of pan-IR700 i.v., 60 J cm^{-2} NIR light (NIR-PIT, n = 3). Pan-IR700 was injected into all mice 24 h before NIR light irradiation. The 60 J cm^{-2} NIR light via a laser (B&W TEK Inc.) was administered to tumor mice with the remainder of the mouse covered with aluminum foil. During the experiments, mice urine samples were gathered as follows: (1) from 25 to 24 h before NIR-PIT (−24 h); (2) from 1 h before NIR-PIT to just before NIR-PIT (0 h); (3) from immediately after NIR-PIT to 1 h after NIR-PIT (1 h); (4) from 1 to 2 h after NIR-PIT (2 h); and (5) from 2 to 3 h after NIR-PIT (3 h). Each mouse was placed on a separate plastic tray, and the urine was collected by micropipette as soon as it dropped on the tray. The urine volume was first measured, and then diluted with purified water in a measuring cylinder to 500 μL total. Each sample was diluted 10 times with 1% (v/v) formic acid in methanol. After centrifugation at 14 000 rpm at 4 °C for 10 min, the supernatants were transferred into new tubes. LCMS analysis was performed on a liquid chromatograph mass spectrometer (LCMS-8050, Shimadzu Co.) as mentioned above. Peak areas of the characteristic peak in the released ligands were calculated from each chromatogram by LabSolutions LCMS software (Shimadzu Co.). For semiquantitative analysis, relative ligand amount was calculated as the product of peak area and urine volume.

Statistics. Data are expressed as means ± SEM from a minimum of three experiments, unless otherwise indicated. Statistical analyses were performed with a statistics program (GraphPad Prism; GraphPad Software). For two group comparisons, the unpaired t test was used. For multiple group comparisons, a one-way analysis of variance (ANOVA) with Tukey's test or Dunnett's test was used. The correlation coefficient was obtained with Peason's product moment correlation coefficient. $P < 0.05$ was considered to indicate a statistically significant difference.

■ ASSOCIATED CONTENT

Supporting Information

The Supporting Information is available free of charge on the ACS Publications website at DOI: 10.1021/acscentsci.8b00565.

Additional figures including ligand release, particle distribution, cell death, correlations, and ^{1}H NMR spectra (PDF)

DOI: 10.1021/acscentsci.8b00565
ACS Cent. Sci. 2018, 4, 1559−1569

Morphological changes of NIR-PIT-treated cells (AVI)
Morphological changes of NIR-PIT-treated cells (AVI)
Morphological changes of NIR-PIT-treated cells (AVI)

AUTHOR INFORMATION

Corresponding Author

*Phone: 240-858-3069. Fax: 240-541-4527. E-mail: kobayash@mail.nih.gov.

ORCID

Hirofumi Hanaoka: 0000-0003-2421-7397
Hisataka Kobayashi: 0000-0003-1019-4112

Author Contributions

K.S. designed and mainly conducted the experiments, performed the analysis, and wrote the manuscript. K.A. and H.T. performed chemical experiments. S.M. and R.K. performed AFM experiments. S.T. performed analysis of the aggregates. H.H. performed biodistribution analysis. T.O. and M.N. did mass spectrometry analysis. S.O., T.N., and M.N. performed in vivo ligand excretion analysis. P.L.C. and Y.H. wrote the manuscript. M.O. supervised chemical experiments, and H.K. supervised, planned, and initiated the project, designed experiments, wrote the manuscript, and supervised the entire project.

Funding

This research was supported by the Intramural Research Program of the National Institutes of Health, National Cancer Institute, Center for Cancer Research. K.S. is supported by the Program for Developing Next-generation Researchers (Japan Science and Technology Agency), KAKEN (18K15923, JSPS), Konica Minolta Science and Technology Foundation, Medical Research Encouragement Prize of The Japan Medical Association, The Uehara Memorial Foundation, Kudo Foundation, Takeda Science Foundation, The Nitto Foundation, Kanae Foundaton for the Promotion of Medical Science, Kowa Life Science Foundation, Shimadzu Foundation, Nakatani-Foundation, the Noguchi Institute, the Asahi Glass Foundation, the Ito Chubei Foundation, and the Murata Science Foundation.

Notes

The authors declare no competing financial interest.
Safety statement: no unexpected or unusually high safety hazards were encountered.

ACKNOWLEDGMENTS

We thank Shimadzu Corporation for providing access and expertise to operate various analytic devices used in this study.

REFERENCES

(1) Mitsunaga, M.; Ogawa, M.; Kosaka, N.; Rosenblum, L. T.; Choyke, P. L.; Kobayashi, H. Cancer Cell-Selective in Vivo near Infrared Photoimmunotherapy Targeting Specific Membrane Molecules. *Nat. Med.* **2011**, *17* (12), 1685−1691.

(2) Sato, K.; Sato, N.; Xu, B.; Nakamura, Y.; Nagaya, T.; Choyke, P. L.; Hasegawa, Y.; Kobayashi, H. Spatially Selective Depletion of Tumor-Associated Regulatory T Cells with near-Infrared Photoimmunotherapy. *Sci. Transl. Med.* **2016**, *8* (352), 352ra110.

(3) Shirasu, N.; Yamada, H.; Shibaguchi, H.; Kuroki, M.; Kuroki, M. Potent and Specific Antitumor Effect of CEA-Targeted Photoimmunotherapy. *Int. J. Cancer* **2014**, *135* (11), 2697−2710.

(4) Jing, H.; Weidensteiner, C.; Reichardt, W.; Gaedicke, S.; Zhu, X.; Grosu, A. L.; Kobayashi, H.; Niedermann, G. Imaging and Selective Elimination of Glioblastoma Stem Cells with Theranostic Near-Infrared-Labeled CD133-Specific Antibodies. *Theranostics* **2016**, *6* (6), 862−874.

(5) Nagaya, T.; Nakamura, Y.; Sato, K.; Harada, T.; Choyke, P. L.; Hodge, J. W.; Schlom, J.; Kobayashi, H. Near Infrared Photoimmunotherapy with Avelumab, an Anti-Programmed Death-Ligand 1 (PD-L1) Antibody. *Oncotarget* **2017**, *8* (5), 8807−8817.

(6) Nakamura, Y.; Nagaya, T.; Sato, K.; Harada, T.; Okuyama, S.; Choyke, P. L.; Yamauchi, T.; Kobayashi, H. Alterations of Filopodia by near Infrared Photoimmunotherapy: Evaluation with 3D Low-Coherent Quantitative Phase Microscopy. *Biomed. Opt. Express* **2016**, *7* (7), 2738−2748.

(7) Ogata, F.; Nagaya, T.; Okuyama, S.; Maruoka, Y.; Choyke, P. L.; Yamauchi, T.; Kobayashi, H. Dynamic Changes in the Cell Membrane on Three Dimensional Low Coherent Quantitative Phase Microscopy (3D LC-QPM) after Treatment with the near Infrared Photoimmunotherapy. *Oncotarget* **2017**, *8* (61), 104295−104302.

(8) Ogawa, M.; Tomita, Y.; Nakamura, Y.; Lee, M.-J.; Lee, S.; Tomita, S.; Nagaya, T.; Sato, K.; Yamauchi, T.; Iwai, H.; et al. Immunogenic Cancer Cell Death Selectively Induced by near Infrared Photoimmunotherapy Initiates Host Tumor Immunity. *Oncotarget* **2017**, *8* (6), 10425−10436.

(9) Sato, K.; Nakajima, T.; Choyke, P. L.; Kobayashi, H. Selective Cell Elimination in Vitro and in Vivo from Tissues and Tumors Using Antibodies Conjugated with a near Infrared Phthalocyanine. *RSC Adv.* **2015**, *5*, 25105−25114.

(10) Sato, K.; Nagaya, T. Near Infrared Photoimmunotherapy Prevents Lung Cancer Metastases in a Murine Model. *Oncotarget* **2015**, *6* (23), 19747−19758.

(11) Castano, A. P.; Mroz, P.; Hamblin, M. R. Photodynamic Therapy and Anti-Tumour Immunity. *Nat. Rev. Cancer* **2006**, *6* (7), 535−545.

(12) Agostinis, P.; Berg, K.; Cengel, K. a; Foster, T. H.; Girotti, A. W.; Gollnick, S. O.; Hahn, S. M.; Hamblin, M. R.; Juzeniene, A.; Kessel, D.; et al. Photodynamic Therapy of Cancer: An Update. *Ca-Cancer J. Clin.* **2011**, *61* (4), 250−281.

(13) Brown, S. B.; Brown, E. A.; Walker, I. The Present and Future Role of Photodynamic Therapy in Cancer Treatment. *Lancet Oncol.* **2004**, *5* (8), 497−508.

(14) Li, X.; Lee, S.; Yoon, J. Supramolecular Photosensitizers Rejuvenate Photodynamic Therapy. *Chem. Soc. Rev.* **2018**, *47* (4), 1174−1188.

(15) Sato, K.; Watanabe, R.; Hanaoka, H.; Nakajima, T.; Choyke, P. L.; Kobayashi, H. Comparative Effectiveness of Light Emitting Diodes (LEDs) and Lasers in near Infrared Photoimmunotherapy. *Oncotarget* **2016**, *7* (12), 14324−14335.

(16) Anderson, E. D.; Gorka, A. P.; Schnermann, M. J. Near-Infrared Uncaging or Photosensitizing Dictated by Oxygen Tension. *Nat. Commun.* **2016**, *7*, 13378.

(17) Anderson, E. D.; Sova, S.; Ivanic, J.; Kelly, L.; Schnermann, M. J. Defining the Conditional Basis of Silicon Phthalocyanine Near-IR Ligand Exchange. *Phys. Chem. Chem. Phys.* **2018**, *20* (28), 19030−19036.

(18) Jin, J.; Krishnamachary, B.; Mironchik, Y.; Kobayashi, H.; Bhujwalla, Z. M. Phototheranostics of CD44-Positive Cell Populations in Triple Negative Breast Cancer. *Sci. Rep.* **2016**, *6*, 1−12.

(19) Davison, J. B.; Wynne, K. J. Silicon Phthalocyanine-Siloxane Polymers: Synthesis and ^{1}H Nuclear Magnetic Resonance Study. *Macromolecules* **1978**, *11* (1), 186−191.

(20) Anula, H. M.; Berlin, J. C.; Wu, H.; Li, Y. S.; Peng, X.; Kenney, M. E.; Rodgers, M. A. J. Synthesis and Photophysical Properties of Silicon Phthalocyanines with Axial Siloxy Ligands Bearing Alkylamine Termini. *J. Phys. Chem. A* **2006**, *110* (15), 5215−5223.

(21) Sato, K.; Watanabe, R.; Hanaoka, H.; Harada, T.; Nakajima, T.; Kim, I.; Paik, C. H.; Choyke, P. L.; Kobayashi, H. Photoimmunotherapy: Comparative Effectiveness of Two Monoclonal Antibodies Targeting the Epidermal Growth Factor Receptor. *Mol. Oncol.* **2014**, *8* (3), 620−632.

(22) Sato, K.; Nagaya, T.; Choyke, P. L.; Kobayashi, H. Near Infrared Photoimmunotherapy in the Treatment of Pleural Dissemi-

DOI: 10.1021/acscentsci.8b00565
ACS Cent. Sci. 2018, 4, 1559−1569

nated NSCLC: Preclinical Experience. *Theranostics* **2015**, *5* (7), 698−709.
(23) Sato, K.; Nagaya, T.; Mitsunaga, M.; Choyke, P. L.; Kobayashi, H. Near Infrared Photoimmunotherapy for Lung Metastases. *Cancer Lett.* **2015**, *365* (1), 112−121.
(24) Ido, S.; Kimiya, H.; Kobayashi, K.; Kominami, H.; Matsushige, K.; Yamada, H. Immunoactive Two-Dimensional Self-Assembly of Monoclonal Antibodies in Aqueous Solution Revealed by Atomic Force Microscopy. *Nat. Mater.* **2014**, *13* (3), 264−270.

DOI: 10.1021/acscentsci.8b00565
ACS Cent. Sci. 2018, 4, 1559−1569